Bioactive Materials 7 (2022) 98–111

Contents lists available at ScienceDirect

Bioactive Materials

journal homepage: www.sciencedirect.com/journal/bioactive-materials

An injectable, self-healing, electroconductive extracellular matrix-based hydrogel for enhancing tissue repair after traumatic spinal cord injury

Yian Luo [a,1], Lei Fan [b,1], Can Liu [c,1], Huiquan Wen [d], Shihuan Wang [e], Pengfei Guan [f], Dafu Chen [g], Chengyun Ning [b], Lei Zhou [a,b,*], Guoxin Tan [a,**]

[a] School of Chemical Engineering and Light Industry, Guangdong University of Technology, Guangzhou, 510006, China
[b] School of Materials Science and Engineering, National Engineering Research Center for Tissue Restoration and Reconstruction, South China University of Technology, Guangzhou, 510641, China
[c] Department of Orthopedic Surgery, The First Affiliated Hospital, Zhejiang University School of Medicine, Hangzhou, 310003, China
[d] Department of Radiology, The Third Affiliated Hospital of Sun Yat-Sen University, Guangzhou, 510630, Guangdong Province, China
[e] Department of Child Developmental & Behavioral Center, The Third Affiliated Hospital of Sun Yat-sen University, Guangzhou, 510630, China
[f] Department of Spine Surgery, The Third Affiliated Hospital of Sun Yat-sen University, Guangzhou, 510630, China
[g] Beijing Research Institute of Traumatology and Orthopaedics, Beijing Jishuitan Hospital, Beijing, 100035, China

ARTICLE INFO

Keywords:
Hydrogel
Injectability
Self-healing
Conductivity
Traumatic spinal cord injury

ABSTRACT

Injectable biomaterial-based treatment is a promising strategy to enhance tissue repair after traumatic spinal cord injury (SCI) by bridging cavity spaces. However, there are limited reports of injectable, electroconductive hydrogels with self-healing properties being employed for the treatment of traumatic SCI. Hence, a natural extracellular matrix (ECM) biopolymer (chondroitin sulphate and gelatin)-based hydrogel containing polypyrrole, which imparted electroconductive properties, is developed for traumatic SCI repair. The resulting hydrogels showed mechanical (~928 Pa) and conductive properties (4.49 mS/cm) similar to natural spinal cord tissues. Moreover, the hydrogels exhibited shear-thinning and self-healing abilities, which allows it to be effectively injected into the injury site and to fill the lesion cavity to accelerate the tissue repair of traumatic SCI. *In vitro,* electroconductive ECM hydrogels promoted neuronal differentiation, enhanced axon outgrowth, and inhibited astrocyte differentiation. The electroconductive ECM hydrogel activated endogenous neural stem cell neurogenesis *in vivo* ($n = 6$), and induced myelinated axon regeneration into the lesion site via activation of the PI3K/AKT and MEK/ERK pathways, thereby achieving significant locomotor function restoration in rats with spinal cord injury ($p < 0.001$, compared to SCI group). Overall, the injectable self-healing electroconductive ECM-based hydrogels developed in this study are ideal biomaterials for treatment of traumatic SCI.

1. Introduction

Traumatic spinal cord injury (SCI) results from a direct and instant mechanical insult to the spinal cord, which causes eternal motor deficits (weakness or paralysis), sensory impairments, and autonomic dysfunction [1]. A progressive cascade of pathophysiological events that result in extracellular matrix (ECM) degeneration, such as inflammation, neuronal damage, and death, eventually cause cystic cavity formation. The cavity blocks the infiltration of cellular elements and regeneration of axons, which finally became a major obstacle for neural regeneration following traumatic SCI [2,3]. Moreover, the formation of cystic cavities affects electrical signal transduction and stimulation of spinal cord tissue, thus affecting the differentiation of neural stem cells and axon regeneration. Several strategies, including stimulation of cell differentiation and neurite growth for neuroregeneration, as well as neuroprotective inflammation, are key points for the efficient repair of traumatic SCI. Nevertheless, these current treatments are effective in only one aspect of this complex and multifaceted disease, and have only limited therapeutic efficacy [4]. Therefore, new multifunctional therapeutic strategies with advanced therapeutic efficacy are being actively

Peer review under responsibility of KeAi Communications Co., Ltd.
* Corresponding author.
** Corresponding author.
E-mail addresses: zhoul@scut.edu.cn (L. Zhou), tangx@gdut.edu.cn (G. Tan).
[1] These authors contributed equally to the work.

https://doi.org/10.1016/j.bioactmat.2021.05.039
Received 3 March 2021; Received in revised form 16 May 2021; Accepted 21 May 2021
Available online 1 June 2021

pursued [5].

Currently, biomaterials and tissue engineering approaches are promising strategies to treat traumatic SCI. ECM hydrogels with biochemical and biophysical properties similar to native brain/spinal cord ECM may be employed to promote tissue repair and regeneration [6–9]. The mechanical properties of ECM hydrogels can be tailored, in some cases, to resemble a range of natural nerve tissues and to modulate stem cell proliferation and differentiation [10,11]. The 3D networks of ECM hydrogels, which have a high water content and highly porous structure, facilitate the transport of oxygen and nutrients. In particular, some injectable ECM hydrogels have been developed to treat traumatically injured spinal cord, as they can effectively fill the lesion cavity and conform to the shape of the defect, thereby seamlessly integrating with the host tissue [12,13]. Further experiments have indicated that the injectable ECM hydrogel supports or promotes axon regeneration via ECM remodelling [14,15]. Another advantage of injectable hydrogels is that they can be injected into targeted areas or tissues directly through minimally invasive techniques that avoid secondary damage [16–19]. ECM hydrogels with self-healing properties have attracted increasing attention in biomedical fields because self-healing is one of the fundamental properties of living tissues. The self-healing ability of hydrogels with dynamic reversible crosslinks allows them to recover their structures and functionalities after injection [20,21]. Moreover, the self-healing ability of hydrogels greatly extends their lifespan *in vivo* [22]. However, only a few reports have shown that injectable self-healing hydrogels can be employed for repairing spinal cord tissue injury *in vivo* [23].

In the nervous system, communication between neurons and other cells occur via electrical signals, which contributes toward neural development, maturation, and tissue regeneration. Signal transmission between cells occurs mainly through the ECM. Combining the electroconductive matrix into the cellular microenvironment facilitates the transmission of intercellular electrical signals between cells. Thus, stimulation and transmission of electrical signals are essential for neuronal functions. Biocompatible electroconductive biomaterials that promote the regeneration of nerve tissues have been widely studied [24]. In our previous studies, we developed a soft, highly conductive hydrogel cross-linked and doped with polypyrrole (Ppy) chains and showed that it accelerates the differentiation of neural stem cells and activates endogenous neural stem cell (NSC) neurogenesis to stimulate tissue repair following traumatic SCI [25]. Hence, the design of hydrogel materials may offer new treatment modalities for traumatic SCI therapy as it simultaneously combines the advantages of injectability, self-healing, biocompatibility, and conductivity, but such research is still lacking.

In this study, we developed injectable, self-healing, and electroconductive ECM-based hydrogels by simply mixing borax-functionalized oxidized chondroitin sulphate (BOC), BOC-doped polypyrrole (BOCP), and gelatin (Gel) under physiological conditions. The hydrogel is formed by dynamic covalent chemistry (Schiff-base and borate-diol ester bonds) and noncovalent electrostatic interaction. Chondroitin sulphate (CS) and gelatin (Gel) are fundamental components of the ECM in the central nervous system (CNS) [26,27]. In particular, CS plays an important role in axonal guidance during embryonic CNS formation [28]. Moreover, pendant sulfonate groups of the CS could potentially serve as strongly acidic doping groups for doping the conducting polypyrrole chains [29]. By adjusting the concentration of BOCP, a series of electroconductive ECM hydrogels with different mechanical properties, swelling ratios, and conductive properties were prepared. Electroconductive ECM-based hydrogels display mechanical stability, shear-thinning, and self-healing ability, and can be effectively injected into the injury site and fill the lesion cavity. We demonstrated that the locally injected electroconductive hydrogel effectively promoted endogenous NSC migration and neuronal differentiation while inhibiting astrocyte differentiation. More importantly, multifunctional hydrogels can induce myelinated axon regeneration into the lesion site via activation of the PI3K/AKT and MEK/ERK pathways. Notably, enhanced endogenous NSC migration, neuronal differentiation, and myelinated axon regeneration further reduced the lesion cavity and improved functional recovery in a rat spinal cord contusion model. Overall, our study demonstrated that electroconductive ECM hydrogels may serve as a suitable candidate in clinical treatment applications of traumatic SCI.

2. Experimental section

2.1. Preparation of borax-functionalized oxidized chondroitin sulphate (BOC)

First, 5 g of chondroitin sulphate (CS, Aladdin, Shanghai, China) was dispersed in 80 mL of deionized (DI) water and stirred magnetically for 10 min at 37 °C until it completely dissolved. Then, 1.93 g of sodium periodate (Aladdin, Shanghai, China) was dissolved in 20 mL DI water in a dark environment and this solution was slowly added into the CS solution. The reaction was allowed to proceed at 37 °C for 6 h in the dark with constant stirring. Secondly, 1.91 g of borax ($Na_2B_4O_7{\cdot}10H_2O$, Aladdin, Shanghai, China) was added and the reaction was continued for another 30 min. Five millilitres of ethylene glycol (98%, Macklin, shanghai, China) was added and incubated for 30 min to neutralize the unreacted sodium periodate. Finally, the solution was dialyzed against 3 L of DI water at room temperature for 24 h using a dialysis tube (Shanghai Lvniao Technology Corporation, China) with a molecular weight cut-off (MWCO) of 3500 Da. The DI water was changed every 8 h during dialysis. After completing the dialysis, the dialysate was placed at −80 °C for 24 h and then the dialysate was freeze-dried to borax-functionalized oxidized chondroitin sulphate. The samples were stored at 4 °C until further use.

2.2. Preparation and characterization of BOC-doped polypyrrole (BOCP)

Briefly, BOC was used as a dopant in the polymerization of pyrrole (Py, 99%, Aldrich, St. Louis, MO, USA.). In a typical synthesis reaction, 100 mL of BOC solution (0.2% w/v in DI water) was prepared and cooled to 4 °C. Then, 70 μL of pyrrole was added and stirred magnetically for 10 min until it was well dispersed. Subsequently, 0.62 g (2.3:1 M ratio to the pyrrole) of ferric chloride hexahydrate ($FeCl_3{\cdot}6H_2O$, 98%, Aladdin, Shanghai, China) was added into 5 mL DI water and stirred magnetically. The $FeCl_3{\cdot}6H_2O$ solution was added dropwise into BOC/py solution. The reaction was allowed to proceed for 24 h at 4 °C. The resulting solution was then centrifuged (5000 g, 15 min) and the supernatants were dialyzed against DI water at room temperature for 48 h using a dialysis tube (MWCO of 3500 Da) to remove unreacted monomers. The dialyzed solution was freeze-dried to obtain the BOCP.

2.3. Formation of electroconductive BOC-doped polypyrrole with gelatin (BOCPG) hydrogels

BOC 10% (w/v) was added to 1 mL DI water. Then, a certain amount of BOCP was added to the BOC solution to form solution A. Solution B was prepared by dissolving 30% (w/v) Gel (gel strength ~100 g Bloom, Type B, G108398) in 1 mL of DI water at 60 °C. Solutions A and B were completely mixed and placed in an incubator at 37 °C for 1 day to obtain electroconductive BOCPG hydrogels. Three types of electroconductive hydrogels were fabricated with BOCP contents of 1%, 3%, and 5% (w/v)), which were named BOCPG-1, BOCPG-3, and BOCPG-5, respectively. The BOCG hydrogel was formed without BOCP. Fourier transform infrared (FTIR) spectra were measured with a Thermo Scientific Nicolet IS10 (USA) using CS, BOC, gelatin, polypyrrole, and BOCPG-3 hydrogel powder directly, with air used as the background.

2.4. Morphological characterization

Morphological studies of the samples were performed using scanning

electron microscopy (SEM; ZEISS Ultra 55, Germany). The lyophilized hydrogel was then quenched with liquid nitrogen. All samples were dried with a stream of nitrogen gas and mounted on Al stubs using an Electrodag 502 (Ted Pella, Inc., Redding, CA) conductive carbon adhesive. The samples used for the above tests were prepared by freezing the hydrogel at −60 °C for 1 d and lyophilizing them in a freeze dryer (FD-10, China) for 6 days.

2.5. Mechanical characterization

To characterize the mechanical properties of the hydrogel, a rheological property test was conducted using a rotary rheometer (Physician MCR301, Anton Paar Austria). All samples (3 mm in thickness and 8 mm in diameter) were applied to the lower plate of the rheometer and preheated to a preset temperature (37 °C). The upper plate was immediately brought down to a gap distance of 1 cm to begin the measurement. First, the linear viscoelastic region was determined by the strain amplitude sweep test (0.1–1500%). The strain amplitude sweep measurements were performed at a fixed frequency of 1 Hz. Angular frequency sweep measurements (0.1–100 rad/s) were conducted at a fixed strain of 1%. To assess the self-healing behaviour of the conducting hydrogels, continuous step strain tests were performed with alternating low strain (5%) to high strain (1500%) at a fixed frequency of 1 Hz. The injectability of the hydrogels was characterised using the flow test mode. Shear rate ranges from 0.01 to 10 s^{-1}. All tests were performed at 37 °C and repeated three times. The mechanical properties of all the samples were measured using a dynamic mechanical analysis (DMA) machine (Q800, TA Company, USA) at 37 °C. Hydrogels were placed between two plates of a compression tester and compressed by the upper plate at a strain rate of 1 N/min. The porosity of the hydrogels was measured by ethanol substitution method, it was determined by the amount of ethanol absorbed by dry hydrogels (3 mm in thickness and 8 mm in diameter), after 24 h immersion in ethanol, using the following Equation (1):

$$\text{Porosity}(\%) = \frac{W_2 - W_1}{d_{ethanol} \times V_{hydrogel}} \times 100\% \quad (1)$$

where W_1 is the weight of dry hydrogel and W_2 is the weight of wet hydrogel, $d_{ethanol}$ is the ethanol density at room temperature, $V_{hydrogel}$ is the volume of the wet hydrogel. The $V_{hydrogel}$ was calculated by the actual thickness and diameter of the samples. Test 5 times, calculate the means.

2.6. Conductivity testing

The electrical conductivity of the electroconductive hydrogels was tested using the four-probe method (RTS-8, Guangzhou Four-Point Probe Technology Company, China) with a sourceMeter. To test the conductivity of all the samples, the gel was prepared with a fixed shape (thickness of 3 mm and 8 mm in diameter). First, the samples were placed on a plate, and then the probes were compressed into the hydrogel. We input the height of the sample and selected the appropriate range to obtain the conductivity of the hydrogel. In theory, the conductivity can be calculated using the following Equation (2):

$$\sigma = \frac{1}{Rt} \quad (2)$$

where σ is the conductivity, R is the resistance, and t is the thickness of the sample. Test 5 times, calculate the means.

2.7. Electrochemical measurements

To characterize the electrical properties of the electroconductive hydrogels, cyclic voltammetry (CV) and electrochemical impedance spectroscopy (EIS) were performed. The 100 μL precursor gel solution was rotated onto conductive glass (ITO) and placed in an incubator at 37 °C for 48 h. A three-electrode system consisting of a working electrode (hydrogel around the surface of ITO), reference electrode (a saturated calomel electrode), and counter electrode (a platinum electrode) was applied to the CV test. The working electrode (hydrogel around the surface of ITO) was immersed into the electrolyte solution (1X PBS, pH 7.4), and the potential applied was between −0.5 and 1 V at a sweep rate of 10 mV/s. EIS at frequencies from 0.01 Hz to 100 kHz and an amplitude of 5 mV (Electrochemical Workstation, ZAHNER, Germany) was performed using the same three-electrode system.

2.8. Evaluation of in vitro biocompatibility

NSCs were isolated from the hippocampi of E14 mouse embryos using an established method [30]. Briefly, the isolated NSCs were cultured in DMEM/F12 medium (Sigma-Aldrich) supplemented with 2 mM GlutaMAX (Thermo, USA), B27 nerve supplement (2% Thermo), 20 ng/mL epidermal growth factor (EGF; PeproTech), and 20 ng/mL basic fibroblast growth factor (bFGF, PeproTech) in a humidified 5% CO_2 incubator at 37 °C. The cell culture medium was changed every 3 days. The NSCs were cultured for 7 days and passaged three to four times for further experiments. To assess the biocompatibility and cytotoxicity of BOCG or BOCPG hydrogels, live cell/dead cell staining and cell count Kit-8 (CCK-8 Dojindo, Japan) assay were performed. Briefly, NSCs were cultured on hydrogels for 24 h and stained with ethidium homodimer-1 (Thermo, USA) and calcein-AM (Sigma-Aldrich, USA) for 20 min. The NSCs were seeded on different substrates and the CCK-8 solution was added to the medium at predetermined time points (1, 3, and 7 days). The supernatant (100 μL) was added to 96-well plates, and the optical density (OD) of absorbance (450 nm, wavelength) was measured using a microplate reader (Multiskan FC, Thermo). Cell viability was calculated as the ratio of viable cells cultured on the hydrogel to that on the control plates. Mouse whole blood was used to test the hemocompatibility of BOCG and BOCPG-3 hydrogels according to previously reported protocols. PBS and Triton X-100 solutions were selected as negative and positive controls, respectively. Equal masses of BOCG or BOCPG-3 hydrogel and an equal volume of whole blood were mixed into anticoagulation tubes and incubated for 4 h, followed by centrifugation at 12000*g* for 5 min at 4 °C. The absorbance was measured, and the haemolysis percentage was calculated according to the following Equation (3):

$$\text{Haemolysis}\ (\%) = \frac{\text{Sample absorbance} - \text{Negative control}}{\text{Positive absorbance} - \text{Negative control}} \times 100\% \quad (3)$$

2.9. Gene expression analysis

The total mRNA of the NSCs cultured on different hydrogels was extracted using the Total RNA Kit (Omega, China) and converted into cDNA using the PrimeScript TM RT reagent Kit (Takara). Real-time quantitative PCR (RT-qPCR) was conducted using a LightCycler 480 SYBR Green I Master (Takara). The primer sequences for each gene are listed in Table S1. GAPDH was used as the reference gene. All experiments were repeated three times, and the results were analysed using the $2^{-\Delta\Delta Ct}$ method.

2.10. Western blot analysis

Cells or tissues were dissolved in radioimmunoprecipitation assay buffer (RIPA buffer, CWBIO, China) containing protease and phosphatase inhibitors (Thermo Fisher). Equal amounts of the proteins were subjected to 10% sodium dodecyl sulphate polyacrylamide gel electrophoresis and transferred to polyvinylidene fluoride (PVDF, Millipore) membranes. The PVDF membrane was blocked with 5% skim milk solution and incubated with specific primary antibodies for 12 h at 4 °C. Finally, the PVDF membrane was incubated with secondary antibodies

at room temperature for 2 h. The antibodies used are listed in Table S2. The bands were visualised by enhanced chemiluminescence (ECL, Thermo Fisher, USA) and analysed using ImageJ software (NIH).

2.11. Immunofluorescence (IF) staining and imaging

Cells and injured spinal cords were fixed with 4% paraformaldehyde (PFA, China) for 30 min. After washing with PBS, the samples were incubated with Triton X-100 (0.1%, Sigma-Aldrich) and BSA (6%, Biofroxx, Germany) for 1 h at 37 °C. Subsequently, the samples were incubated for 12 h at 4 °C with the corresponding primary antibodies (Table S2), followed by corresponding secondary antibodies for another 1 h. Finally, the nuclei were stained with Hoechst 33342 (Sigma, USA). Cell cytoskeleton staining was performed using Actin-Tracker Green (Beyotime, China) 7 days after culture to observe cell adhesion and spreading. The confocal images were captured using a Leica LSM 800 confocal microscope (Leica, Germany).

2.12. Ethics statement

All animal experimental protocols were approved by the Animal Care and Use Committee of South China University of Technology and met the requirements of the National Institutes of Health Guide for the Care and Use of Laboratory Animals.

2.13. In vivo degradation and biocompatibility of hydrogels

Adult female Sprague Dawley rats (SD rats, 280–300 g, n = 18) were used to evaluate the biodegradability and biocompatibility of BOCG and BOCPG-3 hydrogels *in vivo*. The BOCG or BOCPG-3 hydrogels were directly injected into the backs of the rats after anesthetization. On days 7, 14, and 21 days post-injection, the tissues around the hydrogels were cut off and immersed in 4% PFA. The tissue was stained with haematoxylin and eosin (HE) for pathological analysis. The thickness of the inflammation layer for each group was analysed using ImageJ software. The biochemical parameters such as serum enzymes: ALT (alanine aminotransferase), AST (aspartate aminotransferase) and TP (total protein) were evaluated by using an automatic biochemical analyzer (Yingnuo, Nanjing, China). All analyses were performed in triplicate for every sample.

2.14. Animals and surgical procedures

Adult female SD rats (280–300 g, n = 24) were randomly divided into four groups: sham group (n = 6), SCI group (n = 6), BOCG group (n = 6), and BOCPG-3 group (n = 6). First, a mixture of xylazine (5 mg/kg) and ketamine (70 mg/kg) was injected into rats intraperitoneally for anaesthesia. A dorsal laminectomy was then performed at the 10th thoracic level, after which the T9-T10 segment of the spinal cord was fully exposed. The contused spinal cord model was established using a 200 kdyn (Infinite Horizon IH-0400 impactor), as previously reported [13]. After contusion, the muscles and skin were closed in the layers. The bladder was emptied twice daily until the rats returned to normal urination. After a week, the traumatic spinal cords were re-exposed, and the hydrogels were directly injected into the lesion site.

2.15. In vivo magnetic resonance imaging and diffusion tensor imaging

At 6 weeks after surgery, rats were anaesthetized and fixed with 3.0 T MRI scanner (Discovery 750, General Electric, USA) in the supine position. Images of sagittal T2-weighted images were acquired using conventional MRI scans. DTI sequence scanning was performed according to a previous report [31]. Images of the sagittal and AP planes were reconstructed using an AW 4.6 workstation (General Electric, USA). The scan parameters were as follows: TR = 3000 ms, Matrix = 192 × 192, Fov = 100 mm, thickness = 1 mm, spacing = 0 mm, NEX = 8 (for T2 weighted scan); TE = 66.6 ms, TR = 3200 ms, BW = 166.7 kHz, Matrix = 96 × 48, Fov = 80 mm, phase Fov = 0.5, thickness = 2 mm, spacing = 0 mm, NEX = 10, b = 800.

2.16. Functional recovery and footprint analysis

Hind limb locomotor function recovery of rats was evaluated weekly by 21-point Basso-Beattie-Bresnahan locomotion testing (BBB) and footprint analysis. The animals were placed in an open field and allowed to walk freely. BBB scores were evaluated after 5 min of observation. In the footprint function, the forelimbs of rats were stained with blue ink, and the hindlimbs were stained with red ink. The rats were then placed into white paper and required to walk straight. Finally, parameters such as the angle of hind paw rotation, relative position (the length between the centre of forepaws and hind paws), stride length, and base of support (the distance between the right and left hind limbs), were measured according to previous reports [14].

2.17. Histological staining

Rats were sacrificed 6 weeks after surgery. The rats were then perfused intracardially with isotonic physiological saline and 4% paraformaldehyde. The injured spinal cords were harvested and cut to a length of 2 cm. Longitudinal sectioning (15 μm thick) was obtained after the spinal cord was embedded in paraffin. The samples were stained with HE and Masson's trichrome staining according to the standard protocol and then imaged using a Nikon E800 upright microscope.

2.18. Statistical analysis

Data were analysed using SPSS version v19.0.0 (IBM, USA). Data were analysed using nonparametric Kruskal-Wallis test or one-way ANOVA with Bonferroni's post-hoc test. Functional tests were analysed by two-way repeated-measures ANOVA comparing groups versus time points followed by post-hoc pairwise multiple comparisons using the Bonferroni method. All data are expressed as the mean ± standard deviation (SD). Error bars indicate SD (*P < 0.05, **P < 0.01, ***P < 0.001). Significance was assigned at $p < 0.001$.

3. Results and discussion

3.1. Synthesis and physical characterization of electroconductive hydrogels

ECM biopolymer based electroconductive hydrogel was synthesized by a hybrid network of BOC-doped polypyrrole (BOCP), borax-functionalized oxidized chondroitin sulphate (BOC), and gelatin (Gel) following the reaction schematic depicted in Fig. 1A. First, aldehyde groups were introduced to CS through a reaction with sodium periodate, as previously reported [32]. Sodium periodate was used as an oxidant to oxidise the adjacent hydroxyl groups present on the backbone of CS polysaccharides into dialdehyde derivatives. Furthermore, in the presence of the crosslinker borax, CS was linked by borate-diol complexation to form BOC (Fig. S1A). Second, The BOCP was polymerized from a mixture of Py monomer and BOC under oxidative conditions ($FeCl_3{\cdot}6H_2O$). In the presence of the dopant BOC, noncovalent ionic interactions were mainly formed between the $-SO_3^-$ of the BOC chain and the $-N^+$ in the pyrrole ring (Fig. S1B). Doping with BOC also governs the intrinsic conductivity of the Ppy. Finally, BOC, BOCP, and Gel were completely mixed at 37 °C (Fig. 1B), and three types of electroconductive BOC/BOCP/Gel (BOCPG) hydrogels were successfully fabricated with BOCP contents of 1%, 3%, and 5% (w/v)), which were named BOCPG-1, BOCPG-3, and BOCPG-5, respectively. As a control, the BOC/Gel (BOCG) hydrogel was formed without BOCP. During the polymerization of the hydrogel, the amino group in the gel and aldehyde group in BOC formed reversible dynamic covalent crosslinking (Schiff

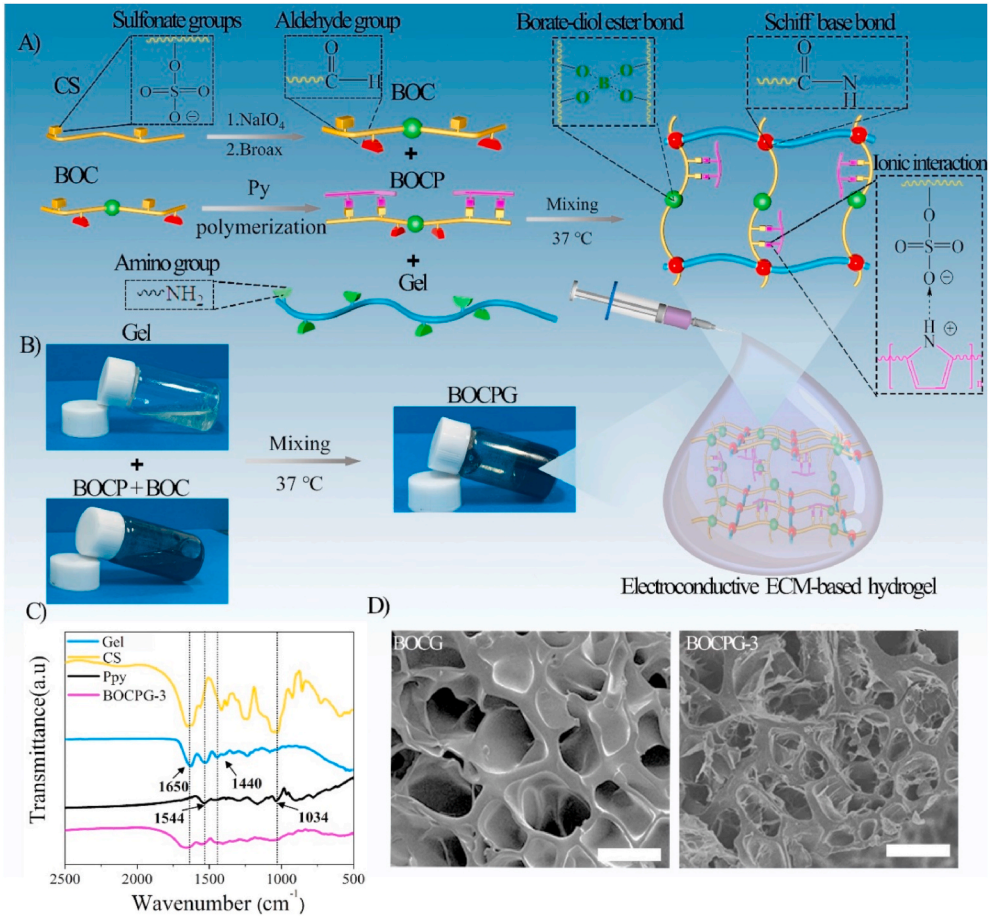

Fig. 1. Characteristics of the dual electroconductive ECM-based hydrogels. A) Schematic of BOC molecule, BOCP and BOCPG formation. The CS is oxidized by $NaIO_4$ to form CS aldehyde molecules. With the introduction of borax molecules, CS aldehyde molecules are cross-linked to formed OC through borate-diol complexation reaction. The synthesis of BOCP by polymerizing Py to form BOCP using BOC as the dopant. BOCPG hydrogel formation by homogeneous mixing of BOC, BOCP, and gelatin (Gel). Photographs show the mixing of BOC, BOCP and Gel to form electroconductive BOCPG hydrogels. C) Fourier transform infrared spectroscopy spectra of CS, Ppy, Gel and BOCPG. D) SEM images of BOCG and BOCPG-3 hydrogels. Scale bar = 25 μm.

base bond), while noncovalent crosslinking was achieved through the electrostatic interactions between the negatively charged BOC and positively charged BOCP. Gel and CS are generally used as the major components of hydrogels owing to their biodegradability and biocompatibility. CS is a major component of the central nervous system and plays an important role in the development of the embryonic nervous system. Although few studies have reported the use of CS chains as biomaterials to promote spinal cord injury repair, it is a promising candidate for the treatment of spinal cord injury. Unlike CS, Ppy is generally used in neural engineering because of its excellent electrical properties and biocompatibility. A previous report has shown that the Ppy polymer can promote the differentiation of NSCs into neurons, improve neuronal outgrowth, and maintain neuronal activity [25,33]. Meanwhile, the introduction of Ppy into the dynamic covalent network of BOCG hydrogel conquers its fast degradability, poor mechanical properties, and provides electrical properties [34]. This is because the PPy polymers were formed through π–π stacking between Ppy chains and ionic interactions with the anionic polymer (BOC). The existence of dynamic covalent cross-linking and non-dynamic covalent cross-linking provides hydrogels with excellent self-healing ability and injectable performance.

The successful preparation of the BOCPG hydrogels was confirmed using Fourier transform infrared spectroscopy. As shown in the FTIR spectrums of CS and OC (Fig. S2A), the peak was observed in the range of 3200–3500 cm^{-1}, which can be attributed to O–H stretching vibrations. Notably, new peaks at 1738 cm^{-1} emerged in the spectrum of OC compared to CS, corresponding to the aldehyde groups. These results show that aldehyde groups were successfully introduced into CS [32]. The characteristic absorption bands for gelatin are located at 1650 cm^{-1} and 1440 cm^{-1} due to the stretching of the C═O bond (amide I) and planar vibration of N–H and C–H (amide III), respectively (Fig. 1C). These peaks were also observed in the BOCPG hydrogels. Meanwhile, the disappearance of 1738 cm^{-1} and a strong peak at 1590–1690 cm^{-1} was observed in the spectrum of BOCPG-3 hydrogels, which suggests the occurrence of Schiff's base reaction. The spectrum of the Ppy powder shows characteristic absorption bands at 1544 cm^{-1} and 1034 cm^{-1}, corresponding to the pyrrole ring vibration and C–H in-plane deformation, respectively [35]. These characteristic absorption bands of pyrrole can be observed in the spectrum of BOCPG-3 hydrogels, indicating that pyrrole was successfully introduced into the BOCPG-3 hydrogel. The microstructures of BOCG and BOCPG-3 hydrogels were observed using scanning electron microscopy (Fig. 1D). The BOCG hydrogels showed microporous network and a smooth surface, which promoted cell adhesion and facilitated cellular penetration. Notably, the porous network structure was maintained in the BOCPG-3 hydrogel with the incorporation of BOCP. The BOCPs are well dispersed alone in the BOCG hydrogel backbone because of the noncovalent ionic interactions between BOC and BOCP. The BOCPG-3 hydrogel exhibited an interconnected porous structure, which facilitated fast electron transmission and enhanced the electrical properties of the BOCPG-3 hydrogels [35]. Thus, our results showed that BOCPG-3 hydrogels were successfully synthesized.

3.2. *Mechanical and electrical characterization of electroconductive hydrogels*

The mechanical properties of a matrix environment are known to affect cell function and differentiation [36]. Dynamic compression tests were performed to assess the elastomeric mechanical performance of the BOCG and BOCPG hydrogels (Fig. 2A). The compressive modulus of all

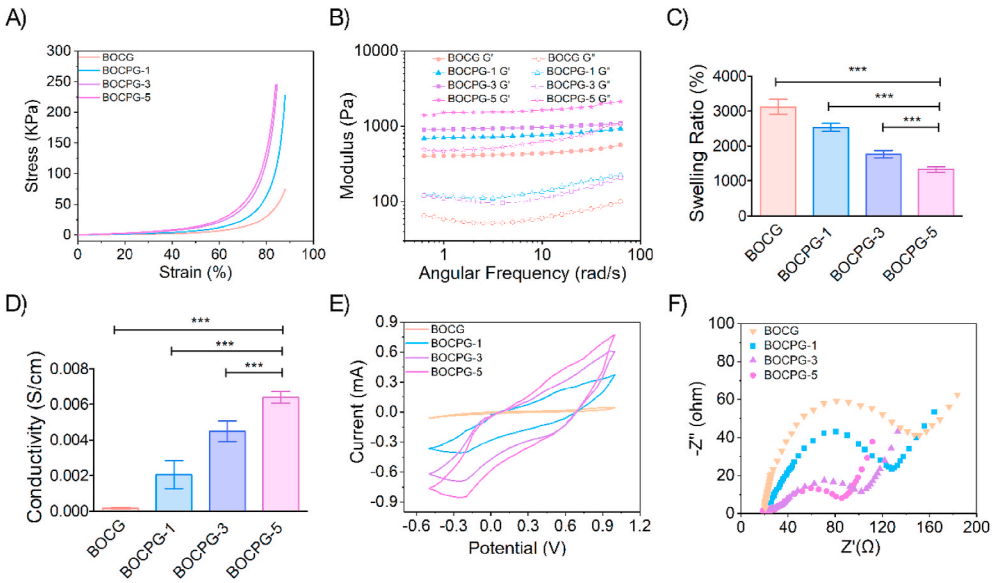

Fig. 2. Physical properties and electrochemical characteristics of the electroconductive hydrogels. A) Stress-strain curves of BOCG hydrogel and different BOCPG electroconductive hydrogels. B) Angular frequency sweep test (0.1–100 rad/s) at a fixed strain (1%) C) Swelling ratio of BOCG hydrogel to different BOCPG electroconductive hydrogels. Error bars indicate SD (*P < 0.05, **P < 0.01, ***P < 0.001, n = 3). D) Conductivity of different hydrogels. (*P < 0.05, **P < 0.01, ***P < 0.001, n = 5). E) Cyclic voltammograms of BOCG hydrogel and different BOCPG hydrogels. F) Nyquist curves of BOCG hydrogel and different BOCPG hydrogels. Error bars indicate the SD (*P < 0.05, **P < 0.01, ***P < 0.001, n = 3).

electroconductive BOCPG hydrogels was higher than that of the BOCG hydrogels. The BOCPG-5 hydrogel exhibited the highest compression modulus (Fig. S4A). To further investigate the mechanical properties of the BOCG and BOCPG hydrogels, a rheological property test was conducted (Fig. 2B). In the angular frequency range (0.1–100 rad/s), the storage modulus (G′) of all groups was higher than the loss modulus (G″), which means that these hydrogels were stable and behaved as viscoelastic solids. As expected, the average storage moduli measured at 10 rad/s increased from 423 ± 40 Pa for BOCG, 686 ± 20 Pa for BOCPG-1, and 928 ± 21 Pa for BOCPG-3 to 1591 ± 66 Pa for BOCPG-5 as the BOCP concentration increased (Fig. S4B). These results show that the incorporation of BOCP into the BOCG hydrogel network could enhance the modulus of electroconductive hydrogels by affecting the crosslinking densities in these hydrogels. Meanwhile, it is well known that π- π conjugation exist in Ppy polymers, which results in rigid products. Hence, the incorporation of BOCP into the BOCG hydrogel network could result in a soft but mechanically stable hydrogels [34]. Notably, BOCPG hydrogels have mechanical properties (100–3000 Pa) similar to natural spinal cord tissue [37]. The effective mass transfer capacity depends on the swelling rate and is crucial for tissue-engineered materials. The maximum swelling ratios of 3121 ± 219%, 2525 ± 114%, 1769 ± 106%, and 1318 ± 82% for BOCG, BOCPG-1, BOCPG-3, and BOCPG-5 hydrogels, respectively, were achieved after 24 h (Fig. 2C). The maximum swelling ratios of all hydrogels decreased with increasing content of BOCP, which can be explained by the fact that the hydrophobic effect of Ppy in the BOCPG hydrogel can influence the swelling ratio. The calculated porosity decreased from 85% for BOCG, 79% for BOCPG-1, 75% for BOCPG-3 and 66% for BOCPG-5 (Fig. S3). The introduction of BOCP into BOCG hydrogel well maintained the interconnected porous structure.

Our previous research suggested that conductive hydrogels have a positive influence on spinal cord injury repair by promoting the transmission of endogenous bioelectrical signals [25]. Therefore, the conductivities of the BOCG and BOCPG hydrogels were measured using the four-probe method. When introducing BOCP with different concentrations of 0%, 1%, 3%, and 5% (w/v), the conductivity of all hydrogels was gradually enhanced to 0.16 ± 0.05, 2.06 ± 0.78, 4.49 ± 0.58, and 6.38 ± 0.33 mS/cm, revealing the contribution of BOCP to the hydrogels' conductivity (Fig. 2D and Table S3). The electronic properties of all groups coated on indium tin oxide (ITO) were investigated by cyclic voltammetry tests in phosphate-buffered saline (PBS; 0.1 M, pH 7.4) versus Ag/AgCl (3 M KCl). As shown in Fig. 2E, a negligible current response was observed in the BOCG groups, whereas a notable current response was observed in all BOCPG groups. All of the BOCPG hydrogels exhibited an anodic peak at 0.53 V and a reduction peak at −0.28 V, and the hysteresis loop had a larger area compared to that of the BOCG hydrogels, which can be attributed to the formation of the Ppy conductive network. The BOCPG-5 hydrogels have the highest current response and area of the hysteresis loop, which indicates that the BOCPG-5 hydrogels are more conductive than the other two BOCPG hydrogels, which is likely due to more π- π conjugation-facilitated electron transport. Electrochemical impedance spectroscopy analyses were also performed to investigate the conductivities of all samples (Fig. 2F). In the Nyquist plots, a semicircle was observed in the high-frequency region for all the groups. The largest diameter of the semicircle was observed in the BOCG group, which implied a high charge-transfer resistance. The diameter of the semicircle decreased in all the BOCPG groups. The diameters of the semicircles of the BOCPG-3 and BOCPG-5 hydrogels were relatively low, indicating the ease of charge transfer. These results were in agreement with the CV results. The low resistance and conductive properties of BOCPG hydrogels are beneficial for neural tissue, which can promote faster cell-cell communication [38]. Among these electroconductive hydrogels, the BOCPG-3 hydrogel, which has intermediate elastic mechanical properties and conductivity similar to the native spinal cord, was selected for further experiments.

3.3. Self-heal ability and injectability of electroconductive hydrogels

The self-healing ability of hydrogels is important for extending their lifetime and recovering their structures and functionalities after injection [22]. Thus, rheological recovery tests were carried out to assess the self-healing properties of the BOCPG-3 hydrogel. First, the strain amplitude sweep measurement of the BOCPG-3 hydrogels was conducted at 37 °C, and the strain ranged from 1% to 1500%. As shown in Fig. S5, the curves of the storage modulus and loss modulus remained stable when the strain was less than 300%. Interestingly, the storage modulus sharply decreased, and the loss modulus increased as the strain increased. The intersection point between the storage modulus and loss modulus was observed when the strain value was 932%. These results indicate that structural destruction of the hydrogel occurred at this point. Subsequently, continuous step strain tests were used to validate the rheological recovery behaviour of the hydrogel (Fig. 3A). The G′ of the BOCPG-3 hydrogels sharply decreased at a high dynamic strain

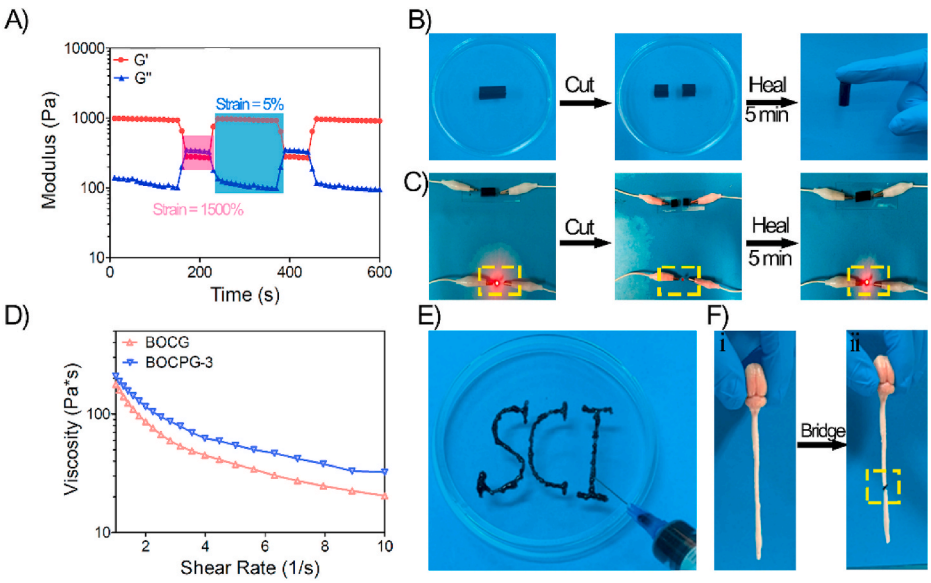

Fig. 3. Multifunctional properties of the electroconductive hydrogels. A) Continuous step strain tests of BOCPG-3 hydrogel with small strain (5%) to big strain (1500%) at 5 Hz frequency at 37 °C. B) The display of self-healing ability of BOCPG-3 hydrogels. The BOCPG-3 hydrogel was cut into two parts and then healed into one again in 5 min at 37 °C. C) The display of the self-healing ability as demonstrated by the electric circuit recovery test. The BOCPG-3 hydrogel served as a conductor to bridge the electric circuit; the LED indicator lit up when external power was supplied. The LED indicator was off when the BOCPG-3 hydrogel was cut off. The LED indicator was lit again when the two pieces of BOCPG-3 hydrogel were put together as they self-recovered into one. D) Viscosity measurement of BOCG and BOCPG-3 hydrogels at 37 °C. E) The injection of BOCPG-3 hydrogel through a syringe. F) (i) Spinal cord of rat, (ii) The spinal cord was cut in the middle and hydrogels were used to bind the spinal cord, demonstrating the adhesive nature of hydrogels.

(1500%), indicating that the structure of the hydrogels was damaged. The value of G′ quickly recovered to the initial value of a low dynamic strain (5%), showing that the hydrogels underwent rapid sol-to-gel transition and the structure was rapidly recovered. These results show that the BOCPG-3 hydrogel has high self-healing efficiency. Macroscopic self-healing tests and electric circuit recovery experiments were also performed to investigate the self-healing ability of the BOCPG-3 hydrogel. As shown in Fig. 3B, the cylindrical BOCPG-3 hydrogel was first cut into two pieces, and the two pieces of hydrogel were put together and placed at 37 °C for 5 min without any external stimulus. Subsequently, the hydrogels healed as a whole and did not break under the force of gravity. In the electric circuit recovery experiment, the LED light was fully recovered after the BOCPG-3 hydrogels underwent a self-healing process (Fig. 3C). The rapid self-healing mechanism of this electroconductive hydrogel was mainly attributed a dynamic reversible covalent Schiff base network between the amine group in gelatin and the aldehyde in BOC. The injectability of the hydrogels was evaluated by viscosity measurements using rheometer at 37 °C. As shown in Fig. 3D, at low shear rate, both BOCPG-3 and BOCG hydrogels had high viscosity. However, with increasing shear rate, BOCPG-3 and BOCG hydrogels showed decreased viscosity. This indicates that both BOCPG-3 and BOCG have good shear thinning capability and were easily injectable. The results also indicate that the addition of BOCP increased the viscosity of the BOCPG-3 hydrogels at higher shear rate. This is mainly attributed to the enhancement of the mechanical properties of the hydrogel after adding BOCP, which was also evident from the above mechanical experiments. The subsequent verification experiment using a 26-gauge needle also indicated the BOCPG-3 hydrogel could be easily injected without clogging (Fig. 3E). Moreover, after injection, the hydrogel regains its structural stability. In addition to self-healing and injectability, BOCPG-3 hydrogels also exhibit excellent adhesive properties. The aldehyde groups in the hydrogel react with amino groups on the tissue surface, as previously reported [39]. As shown in Fig. 3F, the spinal cord was cut into two pieces in the middle, and the BOCPG-3 hydrogels were used as an adhesive to tightly connect the spinal cord to withstand the force of gravity. The self-healing, injectable, and adhesive properties of the BOCPG-3 hydrogel are critical for the application of nerve tissue-engineered materials, as the hydrogel can heal and adhere to the spinal cord at the surgical site after injection.

3.4. *In vitro biocompatibility of the electroconductive hydrogels*

Good biocompatibility is an essential property of tissue engineering materials. The cytotoxicity of BOCG and BOCPG hydrogels was evaluated by Live/Dead staining (Fig. S6A) and cell count Kit-8 (CCK-8) (Fig. S6B). Laser confocal images showed that a significant number of dead cells (red) were not observed in NSCs cultured on different hydrogels. In agreement with the live/dead staining, the CCK-8 assay results showed that the viability of NSCs exceeded 80% for all hydrogels at 1, 3, and 7 days. In addition, hemocompatibility is an important indicator for evaluating the compatibility of implanted materials [40]. Haemolytic activity assays were performed in BOCG and BOCPG-3 hydrogels, in which PBS and Triton X-100 were used as the blank and positive groups, respectively. As shown in Fig. S6C, the solutions of the BOCG and BOCPG-3 groups were light yellow in colour after the hydrogel was co-cultured with the blood solution for 30 min. The solution of the Triton X-100 group was red, which can be explained by the fact that the blood cells were almost ruptured by it. For qualification, the absorbances of the supernatant of all groups were measured to determine the haemolysis ratios. The haemolysis ratios of BOCG and BOCPG-3 hydrogels were 0.71% and 1.47%, respectively, compared to the Triton X-100 group (99%). These results show that all the hydrogels exhibited high biocompatibility for repair applications.

3.5. *In vitro differentiation of NSCs on electroconductive hydrogels*

NSCs have the potential to differentiate into neurons, astrocytes, and oligodendrocytes, and their corresponding markers are β-tubulin III (Tuj1), glial fibrillary acidic protein (GFAP), and myelin basic protein (MBP), respectively [41]. The stem cells were seeded on the surfaces of different samples to determine whether the hydrogels affect the differentiation of NSCs (Fig. 4A). As shown in immunofluorescence (IF) images, compared to nonconductive BOCG hydrogels, all electroconductive BOCPG hydrogels displayed large amounts of Tuj1-positive neurons and MBP-positive oligodendrocytes, with low percentage of GFAP-positive astrocytes. Notably, among all electroconductive hydrogels, BOCPG-3 hydrogels demonstrated extensive neurite outgrowth and a spherical appearance developed by oligodendrocytes. Quantification of IF areas is shown in Fig. 4B. The neurons and oligodendrocytes in the BOCPG-3 hydrogel group were the highest, with an area of 13.36 ± 1.97% and 3.96 ± 0.35%, respectively. However, the astrocytes on the BOCPG-3 hydrogel were 3.15 ± 1.17%, which were lower than that in the BOCG (15.49 ± 0.78%), BOCPG-1 (10.67 ± 0.73%) and BOCPG-5 (6.81 ± 1.55%) groups. Furthermore, Real-time quantitative PCR and WB were conducted to determine the *in vitro* expression of marker genes/proteins in NSCs cultured on different

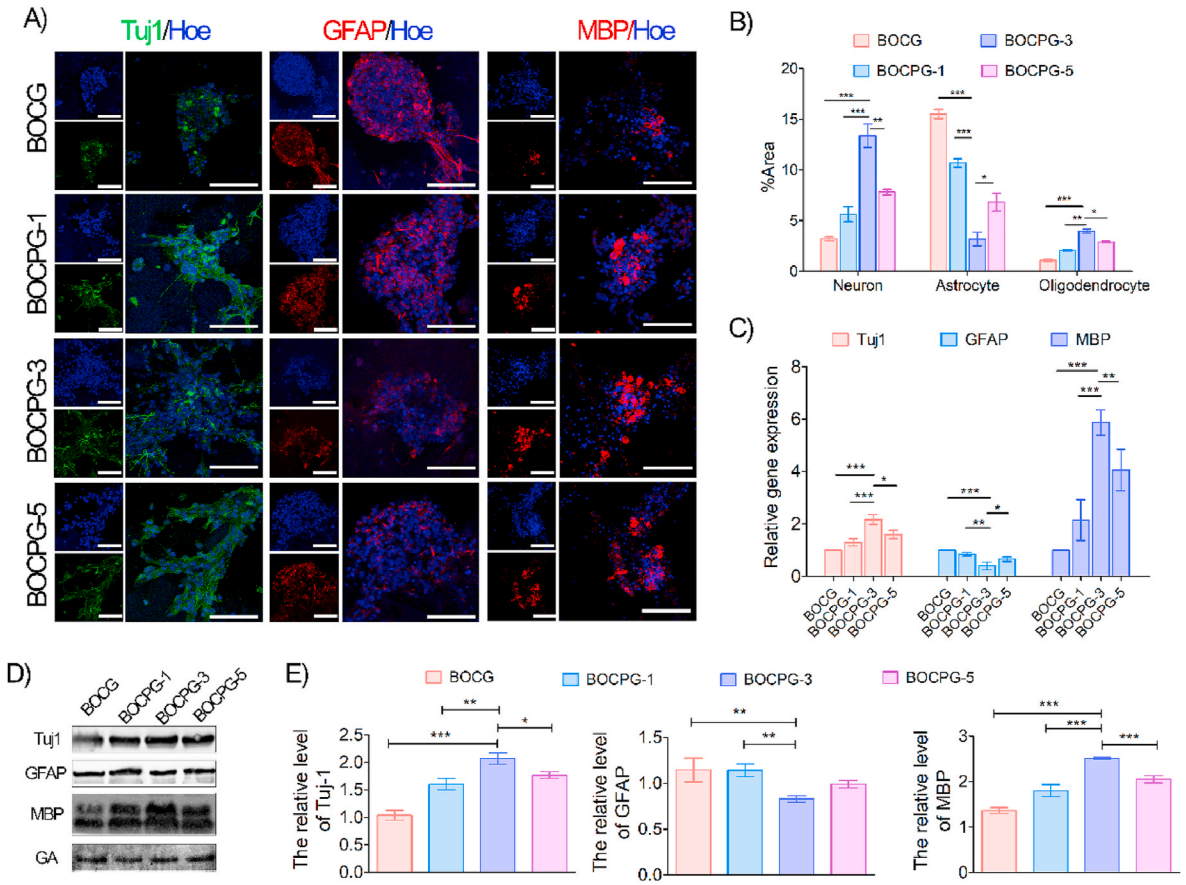

Fig. 4. *In vitro* NSC differentiation on BOCPG hydrogels. A) Confocal microscopy images of NSC differentiation on different hydrogel samples for 7 days. Electroconductive hydrogels can promote the differentiation of NSCs into neurons (green) and oligodendrocytes (red), while inhibiting the differentiation of NSCs into astrocytes (red). The nuclei were stained with Hoechst (blue). Scale bar = 100 μm. B) The illustration shows the quantitative analysis of immunofluorescence intensity. Error bars indicate the SD (*P < 0.05, **P < 0.01, ***P < 0.001, n = 3) C) Gene expression levels of NSCs cultured on different hydrogels. RT-qPCR analysis shows that electroconductive hydrogels promote the expression of Tuj1 and MBP genes and inhibit the expression of GFAP genes in NSCs. Error bars indicate the SD (*P < 0.05, **P < 0.01, ***P < 0.001, n = 3) (D) Protein expression of Tuj1, GFAP, and MBP of NSCs cultured on different samples. E) Quantification of Western blot data. Error bars indicate SD (*P < 0.05, **P < 0.01, ***P < 0.001, n = 3).

samples after 7 days. According to the RT-qPCR analysis (Fig. 4C), all electroconductive BOCPG hydrogels exhibited a higher gene expression of Tuj1 and MBP, but lower expression of GFAP, relative to the non-conductive BOCG group. Among them, the BOCPG-3 group displayed 2.2-fold and 5.8-fold higher Tuj1 and MBP expression than that of the BOCG group, respectively. In contrast, GFAP expression in the BOCPG-3 group was 0.39-fold lower than that in the BOCG group. As shown in the WB assay (Fig. 4D–E), the protein expression of Tuj1, MBP, and GFAP was consistent with their gene expression. These results indicate that NSCs optimally differentiated into neurons and oligodendrocytes, however, they differentiated to a lesser degree into astrocytes in the conductive microenvironment. The electrical microenvironment of a conductive hydrogel can influence developmental events such as neuronal differentiation, migration, and the establishment of a neurotransmitter phenotype by promoting cell-cell communication using bioelectric signals [42,43]. Moreover, soft hydrogels with mechanical properties are similar to native CNS tissue (0.1–16 kPa), which would provide a more suitable environment for survival and neuronal differentiation [25]. Therefore, the BOCPG-3 hydrogel can enhance neuronal activity and neural differentiation, which can be attributed to its lower strength and higher electrical performance.

3.6. *In vitro* NSCs axon outgrowth on electroconductive hydrogels

The axonal growth of endogenous NSCs plays an important role in traumatic SCI repair. To investigate whether electroconductive hydrogels affect the axonal outgrowth of NSCs, cell cytoskeleton (Fig. 5A) and IF staining (Fig. 5B) were performed at 7 days. Compared with the non-conductive BOCG hydrogel, the spreading area and nerve density of NSCs in all electroconductive BOCPG hydrogels were increased. These results proved that the existence of an electrical microenvironment is beneficial for axonal outgrowth. Neuron-specific neurocan (NeuR) and axonal-specific neurofilament (NF) were evaluated by IF labelling and WB analysis. As shown in Fig. 5C, the longest axon length and synaptic network formation was observed in BOCPG-3 hydrogel (113.48 ± 16.21 μm), which was significantly higher than BOCG (24.33 ± 5.29 μm, $p < 0.001$), BOCG-1 (48.21 ± 6.36 μm, $p < 0.001$) and BOCPG-5 (70.29 ± 4.37 μm, $p < 0.001$). The results of WB analysis were in agreement with those of IF staining (Fig. 5D–E). In RT-qPCR evaluation, the relative gene expression of NF and growth associated protein (GAP43) in the BOCPG-3 hydrogel were 5.8 and 2.7 times higher than that of BOCG control group (Fig. 5F). Together, these results showed that the BOCPG-3 hydrogel with high electroactivity and appropriate elasticity can enhance neuronal proliferation and axonal extension, representing a potential mechanism of repair for traumatic SCI [44].

3.7. *In vivo* degradation and biocompatible evaluation of electroconductive hydrogels

The *in vivo* degradation of BOCG and BOCPG-3 hydrogels was performed by direct injection into rat subcutaneous tissue. As shown in

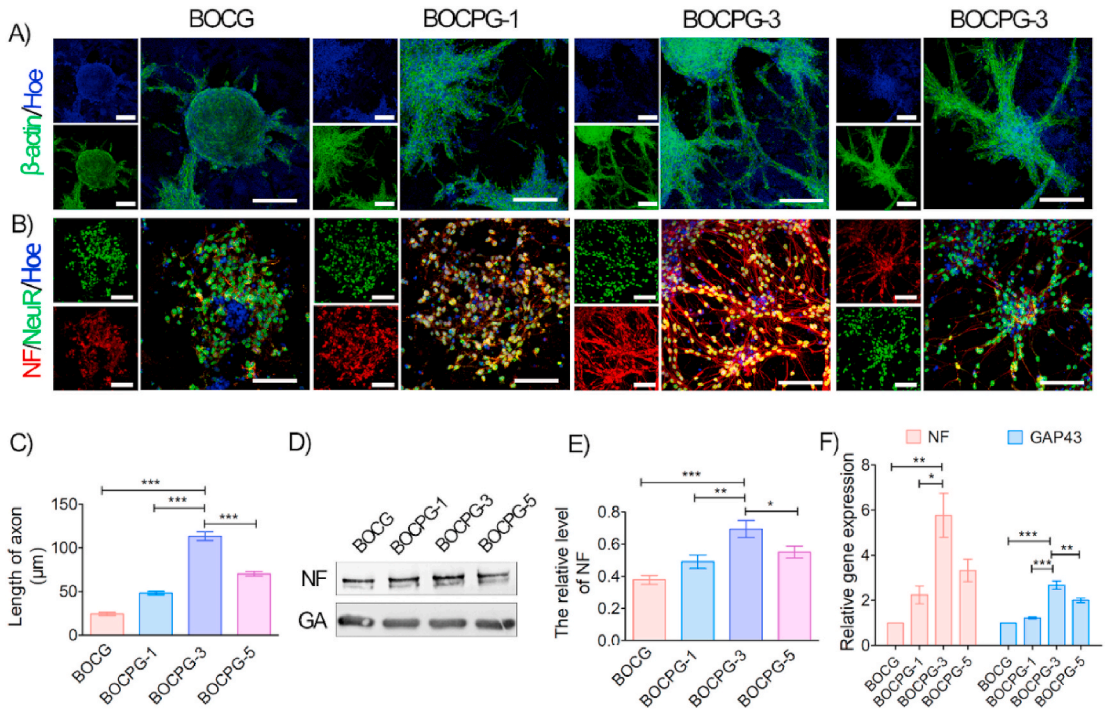

Fig. 5. *In vitro* NSC axon outgrowth on BOCPG hydrogels. A) Cytoskeletons of NSCs cultured on different hydrogel samples for 7 days. The nuclei were stained with Hoechst (blue). Scale bar = 100 μm. B) Confocal microscopy images showed the expression of neurofilament (NF, red) and neuron-specific nuclear protein (NeuN, green) cultured on different samples for 7 days. The nuclei were stained with Hoechst (blue). Scale bar = 200 μm. C) The length of axon of NSCs cultured on different samples. Error bars indicate SD (*P < 0.05, **P < 0.01, ***P < 0.001, n = 9) D) Protein expressions of NF on different groups. E) Quantification of Western blot data. Error bars indicate SD (*P < 0.05, **P < 0.01, ***P < 0.001, n = 3) F) Gene expression levels of NSCs cultured on different hydrogels. Error bars indicate SD (*P < 0.05, **P < 0.01, ***P < 0.001, n = 3). RT-qPCR analysis shows that the electroconductive hydrogels promote the expression of NF and GAP43 genes.

Figs. S7A–B, the hydrogels maintained a hemispherical shape (15 mm ø, 5 mm height) on day 0. The BOCPG-3 hydrogel became smaller and flatter, whereas the BOCG hydrogel completely disappeared at 14 days post-implantation. Over time, only a small amount of the BOCPG-3 hydrogel was observed after 21 days. These results showed that the degradation rate of the BOCG hydrogel was slightly faster than that of the BOCPG-3 hydrogel. BOCPG-3 hydrogel exhibits improved chemical stability (π-π stacking and ionic interaction) compared to BOCG hydrogels due to the incorporation of conductive Ppy [34,45]. HE staining was performed to determine cell infiltration during hydrogel degradation at 7, 14, and 21 days. Seven days post-implantation, numerous macrophages were observed around the hydrogels. As the implantation time increased, the hydrogels gradually eroded and degraded, and a small number of macrophages invaded the interface between the hydrogel and tissue. Meanwhile, a few small BOCP conductive particles were observed at 21 days post-implantation (Fig. S7C). These results can be explained by the fact that the BOCP conductive backbone can be degraded *in vivo*. As shown in Fig. S7D, the thickness of the inflammation layer of the BOCPG-3 group was higher than that of the BOCG group at 7, 14, and 21 days. The thickness of the inflammation layer of the BOCPG-3 group (488.59 ± 24.51 μm) and BOCG group (407.23 ± 14.64 μm) achieved the highest level at 14 days, and gradually decreased. In our previous report, Ppy nanoparticles were confirmed to be a relatively safe conducting polymer material that can be degraded *in vivo* [25]. In addition, the rats treated with BOCG and BOCPG-3 hydrogels did not cause histological damage to major organs (heart, liver, spleen, lung, and kidney), compared to the sham group (Fig. S8A). The levels of aspartate aminotransferase (AST), alanine aminotransferase (ALT), and total protein (TP) in the BOCG and BOCPG-3 hydrogel groups did not show a significant variation compared to the sham group (Figs. S8B–D). Overall, the BOCPG-3 hydrogel showed great promise as a safe biomaterial for the treatment of traumatic SCI due to its biocompatibility.

3.8. Electroconductive hydrogels improved neural pathology and functional recovery

Functional recovery is correlated with the nerve structure and pathophysiology of contusion [46]. It is well known that a cystic cavity is formed and enlarged 1 week after traumatic SCI, followed by progressive secondary damage, including inflammation, oxidative stress, and apoptosis [14]. Therefore, the BOCG and BOCPG-3 hydrogels were injected directly into the cystic cavities after a week to evaluate the therapeutic effect (Fig. 6A). Basso-Beattie-Bresnahan locomotion testing and gait function analyses were assessed 6 weeks after contusion. All rats immediately reached a state of complete hindlimb paralysis post-surgery (BBB score = 1) and gradually recovered in a time-dependent manner (Fig. 6B). Functional recovery was rapidly achieved in the BOCPG-3 group with higher BBB scores (13.2 ± 0.8) than in the BOCG group (11 ± 0.9) and SCI group (9 ± 0.7) on day 42 post-injury. Notably, in comparison with the SCI group, the motor function of rats in the BOCPG-3 and BOCG groups recovered more quickly. Although there is considerable variability in BBB open-field score of individual rats at 21 days after injury, when the group as a whole reaches a functional plateau. However, we repeated the experiment many times to avoid variability in BBB open-field score of individual rats [47]. In representative footprint analysis (Fig. 6C–D), the hind limbs of injured rats in the SCI group were considerably dragged, while the BOCPG-3 group showed clear footprints with no drag lines. For qualification, the mean stride length was 100 ± 7 mm in the BOCPG-3 group higher than 80 ± 4 mm in the BOCG group, which was close to that in the sham-operated group (123 ± 6 mm). The base of support, relative position, and rotation angle dramatically decreased after BOCPG-3 hydrogel treatment. As shown in Fig. 6E–F and Fig. S9, gross anatomy and conventional magnetic resonance imaging (MRI) were conducted to assess the pathology of the injured spinal cord after contusion at 6 weeks. The contusion site in the injured spinal cord displayed prominent irregular cavities and large

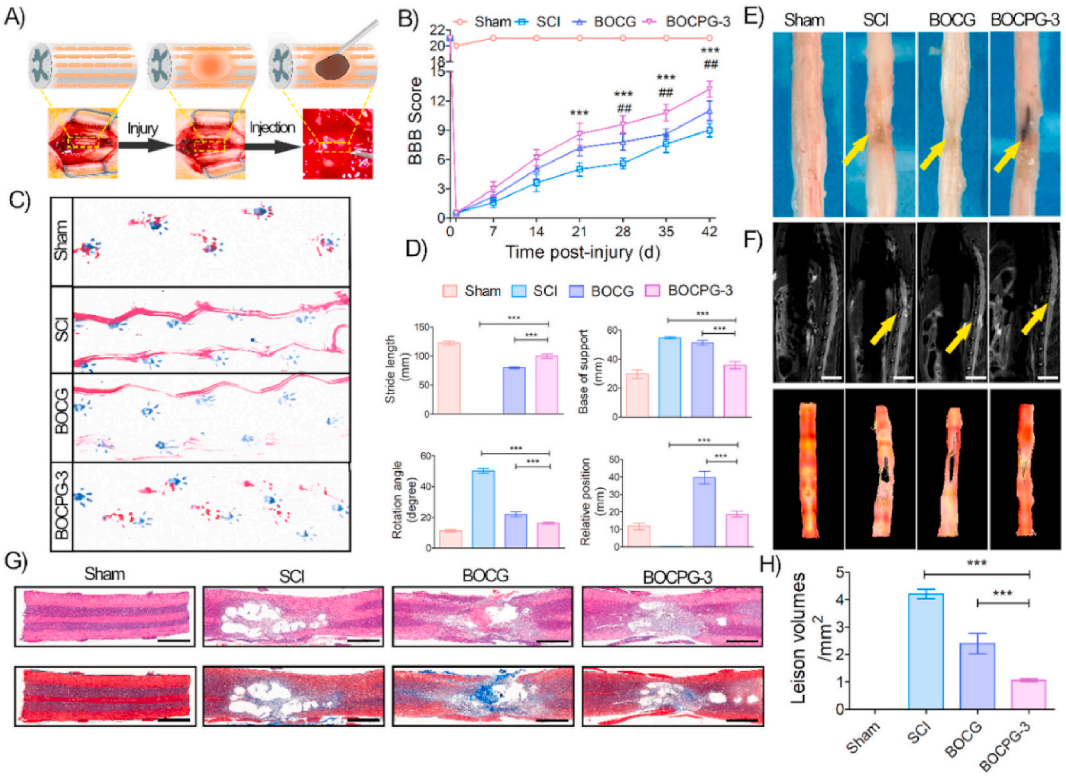

Fig. 6. Injection of BOCPG-3 hydrogel improves functional recovery and reduces the lesion cavity. A) Illustration of the process of traumatic SCI and hydrogel injection. B) Locomotor recovery of rats was evaluated by BBB score on an open field. The rats treated with the BOCPG-3 hydrogel showed improved BBB scores 2 weeks after injury. Error bars indicate standard deviation (SD) (relative to the SCI group * $p < 0.05$, ** $p < 0.01$, *** $p < 0.001$, relative to the BOCG group, $^{\#}p < 0.05$, $^{\#\#}p < 0.01$, $^{\#\#\#}p < 0.001$, (n = 6)). C) The recovery of hind limb motor function in rats of different groups was analysed using representative footprints. The forepaw was stained with red ink, and the hind paw was stained with blue ink. D) Stride length, base of support, rotation angle, and relative position were used to quantify locomotion recovery at 6 weeks after injury. Error bars indicate SD (*P < 0.05, **P < 0.01, ***P < 0.001, n = 3). E) Representative spinal cord images after SCI repair in all groups. Yellow arrows indicate the location of the spinal cord injury. F) Representative MRI and DTI images after spinal cord injury repair in all groups. Yellow arrows indicate the location of the spinal cord injury. The scale of MRI images was 10 mm. G) Representative images of haematoxylin-eosin staining and Masson's trichrome staining show the morphology of the spinal cord in different groups. Scale bar = 2 mm. H) Illustration of lesion volume area. Error bars indicate SD (*P < 0.05, **P < 0.01, ***P < 0.001, n = 3).

fibrous scars, which were caused by the loss of nerve tissue and extracellular matrix [48]. Diffusion tensor imaging (DTI) and MRI images further demonstrated that the cavity in the contusion site became smaller, which can be attributed to the infiltration and growth of nerve fibres. H&E and Mason staining were performed to further visualise the structure and [49] amount of nerve cell infiltration and fibre formation was observed in the BOCPG-3 group. The area of cavities in BOCPG-3 group (1.06 ± 0.07 mm^2) was smaller than that in BOCG (2.39 ± 0.38 mm^2) and SCI groups (4.21 ± 0.18 mm^2). These results suggest that BOCPG-3 hydrogels injected into the traumatic spinal cord can enhance the capacity for tissue regeneration, resulting in distinct coordination and motor recovery.

3.9. Electroconductive hydrogels promotes endogenous neurogenesis

To further investigate the influence of hydrogels on injury reconstruction, local neurogenesis and astrological scar formation were further elucidated at the lesion site of the spinal cord. Neurogenesis includes the migration, proliferation, and neural differentiation of endogenous NSCs. Numerous nestin-positive cells, an indicator of endogenous NSCs, were observed around the edge of the injury site in the BOCPG-3 group, suggesting that endogenous NSCs migrated into the lesion area and differentiated into new neurons (Fig. S10). Importantly, numerous Tuj1 positive cells, newborn neurons of NSCs, were also observed at the site of the lesion and adjacent to it in the BOCPG-3 group, while these cells were relatively scarce in the BOCG hydrogel and SCI groups (Fig. 7A). In contrast, excessive reactive astrocytes gathered around the site of the lesion to form a glial scar, which further inhibits nerve fibre permeation and reconstruction. In magnified views, the SCI group showed significantly high GFAP-positive glial cells in the lesion ($p < 0.001$) and adjacent sites ($p < 0.001$), whereas Tuj1-positive neurons were considerably low, compared with the BOCPG-3 hydrogel. Furthermore, the levels of Tuj1 and GFAP were quantified in terms of the area percentage of the corresponding positive staining (Fig. 7B). For quantification, the GFAP level dramatically increased around the injury site in the SCI group ($44.29 \pm 5.98\%$) compared with the BOCG ($31.46 \pm 6.01\%$) and BOCPG-3 groups ($15.68\% \pm 3.55\%$). However, the ratio of GFAP and Tuj1 was reversed in the BOCPG-3 group, which suggests that the hydrogel treatment induced neuron-like cell accumulation and mitigated the accumulation of astrocytes at the injured site. Furthermore, the lesion and adjacent regions of injured spinal cords were also analysed for the area percentage of Tuj1 and GAFP, which demonstrated the significant regenerative effect of the BOCPG-3 hydrogel (Fig. 7C). As shown in the WB assay (Fig. 7D–E), the protein expression of Tuj1, and GFAP was consistent with IF results. Together, these findings indicate that the BOCPG-3 hydrogel, with excellent conducting electroactive properties, promotes endogenous neurogenesis and axonal outgrowth, and decreases glial scar formation *in vivo*.

3.10. Electroconductive hydrogels promotes axon regeneration and remyelination

Mature nerve fibres and myelin play vital roles in the entire process of SCI and repair. The myelin-associated axon fibres are derived from

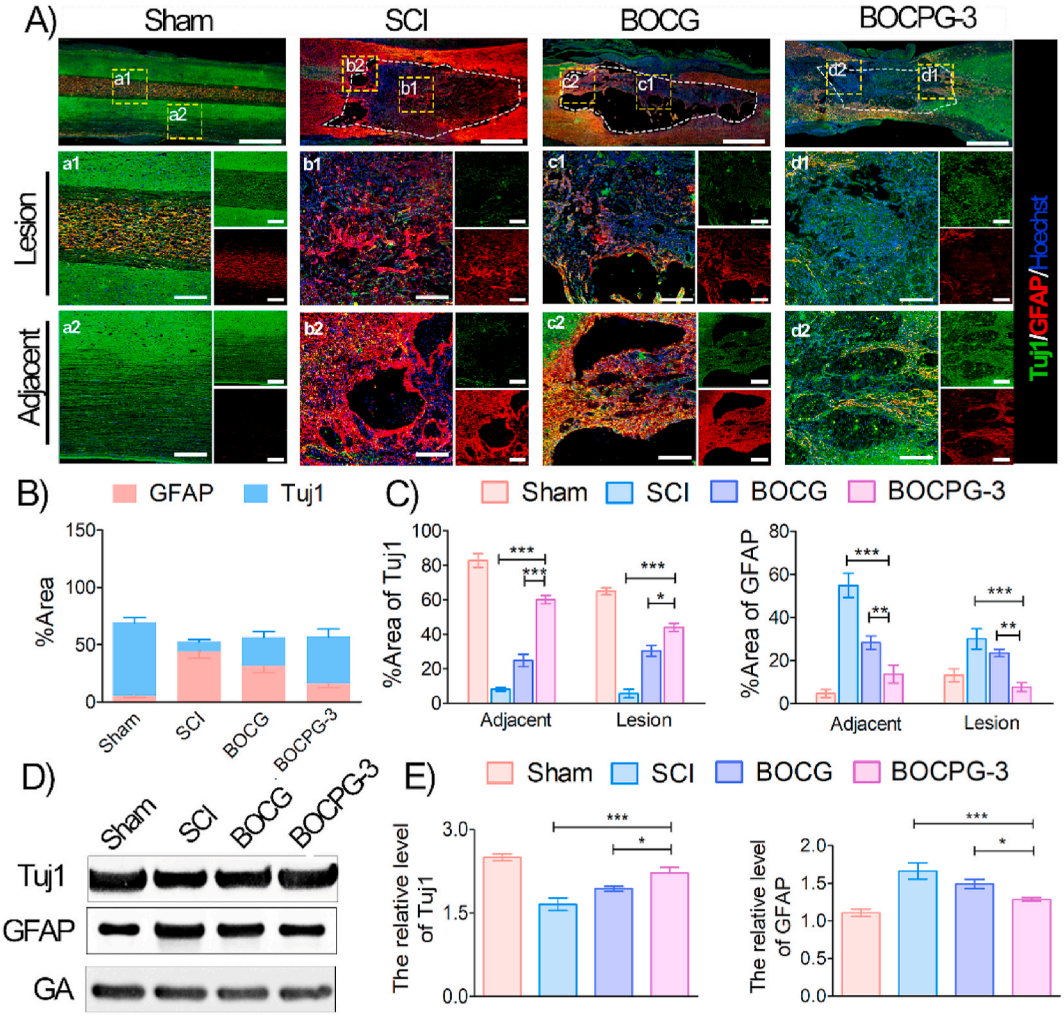

Fig. 7. Injection of BOCPG-3 hydrogel promotes endogenous neurogenesis. A) Representative immunofluorescence images of different groups at 6 weeks. The spinal cords were stained with antibodies against neuronal markers (Tuj1, green) and glial fibrillary acidic protein (GFAP, red). Scale bar = 1 mm. The area surrounded by the white dashed line represents the area of injury to the spinal cord. Boxed regions representing lesions and adjacent regions in each gross immunohistofluorescence image are magnified in a1-a4 and a2-d2, respectively (n = 3). Scale bar = 200 μm. B) The illustration shows the quantitative analysis of immunofluorescence intensity Tuj1 and GFAP in spinal cord tissue (n = 3). C) Redistribution of Tuj1 and GFAP was analysed at the lesion site and adjacent area, respectively. Error bars indicate SD (*P < 0.05, **P < 0.01, ***P < 0.001, n = 3). D) Protein expression of Tuj1 and GFAP. E) Quantification of Western blot data. Error bars indicate SD (*P < 0.05, **P < 0.01, ***P < 0.001, n = 3).

newborn neurons; they invade into cavities and reduce the formation of cavities, thereby forming active connections with neurons at the distal end of injury [50]. As shown in Fig. 8A, the density and number of punctate axonal fibres were barely detected in lesions and adjacent regions in the SCI group, which can be explained by the inhibition of the growth of nerve fibres by glial scars. In contrast, consecutive and larger degrees of NF-positive fibre infiltration were observed in the BOCPG-3 hydrogel. Notably, the density of the MBP-positive myelin sheath was significantly higher in the BOCPG-3 group compared to the SCI group ($p < 0.001$), suggesting that axons are typically wrapped with myelin sheets. The area ratios of NF and MBP in the lesion site were both increased by the BOCPG-3 hydrogel, at 41.26 ± 7.29% and 8.21 ± 2.09%, respectively (Fig. 8B). Moreover, the area percentages of NF and MBP were quantified in the lesion and adjacent regions of the injured spinal cord (Fig. 8C). These results strongly indicate that the electroconductive hydrogel significantly improved myelinated nerve fibres. In addition, enhanced myelin-associated axon regeneration after hydrogel implantation were also observed by analysis of NF, and MBP protein levels by western blotting (Fig. 8D–E). As the BOCPG-3 hydrogel promotes neural regeneration, it may contribute to the electroconductive hydrogel bridge and restore the injured spinal circuit in the lesion area, thereby delivering endogenous electrical signals to the interrupted cells. Furthermore, the presence of endogenous bioelectric cues and ECM in the lesion promoted the formation of neural networks that might connect severed ascending and descending axons in the injured spinal cord.

BOCPG-3 electroconductive hydrogel treatment prominently exerted a positive effect on nerve regeneration; however, the possible related molecular mechanism is still unknown. The PI3K/AKT and MEK/ERK signal pathway plays an important role in regulating neuronal activity and axonal outgrowth. To investigate the possible mechanism of hydrogel promoting repair of the injured region, the PI3K/AKT and MEK/ERK pathways were examined using western blotting in all groups. Results showed that the p-PI3K, *p*-AKT, *p*-MEK, and *p*-EKK expression levels were relatively higher in the BOCPG-3 and BOCG groups at 6 weeks post-surgery. In contrast, the expression of PI3K/AKT and MEK/ERK was extremely low in the SCI group. The possible molecular mechanism of BOCPG-3 hydrogels promotes axon outgrowth by acting PI3K/AKT/MEK/ERK pathway was shown in Fig. 8F [51]. These findings further demonstrated that the BOCPG-3 hydrogel promoted axon extension and myelination by activating the PI3K/AKT and MEK/ERK pathways. Our results showed that BOCPG-3 hydrogel could promote the recovery of hind limb function in the rat model of spinal cord injury.

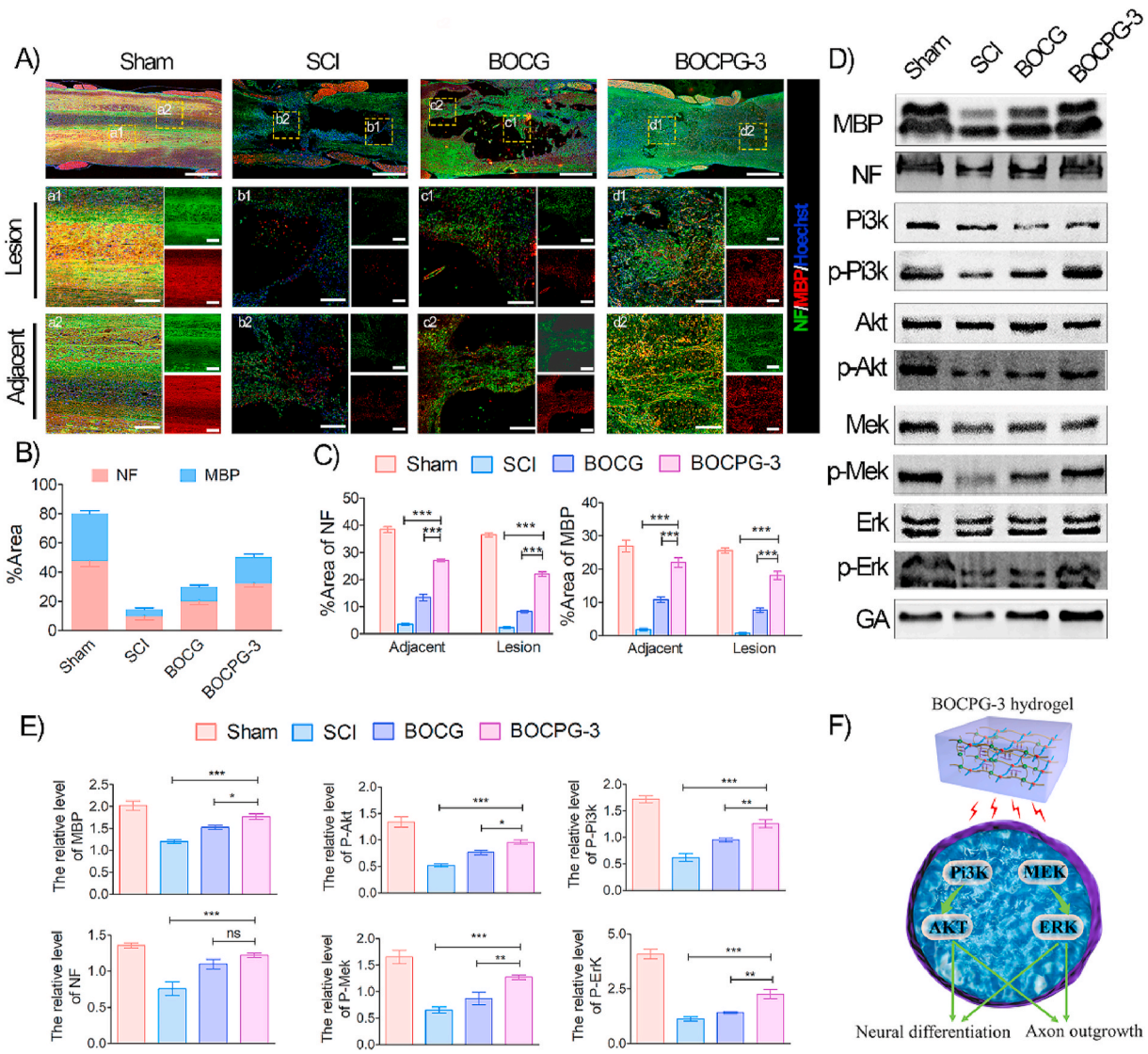

Fig. 8. Injection of BOCPG-3 hydrogel promotes axon regeneration and remyelination. A) Representative immunofluorescence images of different groups at 6 weeks. The spinal cords were stained with antibodies against neurofilament (NF, green) and myelin basic protein (MBP, red). Scale bar = 1 mm. Boxed regions representing lesions and adjacent regions in each gross immunohistofluorescence image are magnified in a1-a4 and a2-d2, respectively. Scale bar = 200 μm n = 3. B) The illustration shows the quantitative analysis of immunofluorescence intensity of NF and MBP in spinal cord tissue (n = 3). C) Redistribution of NF and MBP was analysed at the lesion site and adjacent site, respectively. for the n = 6 micrographs for each group. Error bars indicate SD (*P < 0.05, **P < 0.01, ***P < 0.001, n = 3). D) Protein expression of NF MBP and PI3K/AKT pathway in the different groups. E) Quantification of Western blot data. Error bars indicate SD (*P < 0.05, **P < 0.01, ***P < 0.001, n = 3). F) Illustration showed that the mechanism of BOCPG-3 hydrogels promotes axon outgrowth by acting PI3K/AKT/MEK/ERK pathway.

However, Our future work will focus on longterm human experiment to assess the effect of conductive hydrogel due to species-specific immunological properties.

4. Conclusions

In this study, we developed a biocompatible electroconductive ECM-based BOCPG hydrogel with good injectability and self-healing ability for repairing traumatic SCI. BOCPG hydrogels can be injected into posttraumatic cavities as they induce bridging effects to achieve tissue repair after traumatic SCI. Our *in vitro* results showed that the BOCPG-3 hydrogel could accelerate neuronal and oligodendrocyte differentiation, suppress the differentiation of astrocytes, and enhance axonal growth. Furthermore, our *in vivo* data demonstrated that locally injected conductive hydrogel can serve as a conductive bridge and promote endogenous neural stem cell migration and neuronal differentiation, while inhibiting the formation of glial scars. More importantly, the BOCPG-3 hydrogels can induce myelinated axon regeneration into the lesion site via activation of the PI3K/AKT and MEK/ERK pathways. Finally, the BBB score and representation footprints analyses showed that the BOCPG-3 hydrogels could promote locomotor recovery in rats afflicted with spinal cord injury. This study provides a promising approach to the design of spinal cord tissue engineering materials to treat traumatic SCI by combining electroconductive and biocompatible ECM-based hydrogels.

CRediT authorship contribution statement

Yian Luo: Investigation, Methodology, Formal analysis, Validation. **Lei Fan:** Investigation, Validation. **Can Liu:** Investigation, Formal analysis, Validation, Methodology, Visualization, Writing – review & editing. **Huiquan Wen:** Investigation, Methodology. **Shihuan Wang:** Investigation, Validation, Formal analysis. **Pengfei Guan:** Investigation, Validation, Formal analysis. **Dafu Chen:** Investigation, Formal analysis,

Methodology. **Chengyun Ning:** Funding acquisition, Resources, Project administration. **Lei Zhou:** Funding acquisition, Resources, Project administration, Supervision, Conceptualization, Methodology, Visualization, Investigation, Formal analysis, Validation, Writing – original draft, Writing – review & editing. **Guoxin Tan:** Funding acquisition, Resources, Project administration, Supervision, Conceptualization, Methodology, Visualization, Investigation, Formal analysis, Validation, Writing – original draft, Writing – review & editing.

Declaration of competing interest

The authors declare that they have no known competing financial interests or personal relationships that could have appeared to influence the work reported in this paper.

Acknowledgements

We thank L. Fan for his help in drawing the schematic diagram and typesetting figures. This work was supported by the National Natural Science Foundation of China (Nos. 51932002, 51903087, and 31771080), the Science and Technology Innovation Team Project of Foshan (No. 2018IT100101), Sino-Singapore International Joint Research Institute (No. 203-A018004), and the Joint Fund of Ministry of Education for Equipment Preresearch (No. 6141A02022632).

Appendix A. Supplementary data

Supplementary data to this article can be found online at https://doi.org/10.1016/j.bioactmat.2021.05.039.

Data availability statement

The data that support the findings of this study are available from the corresponding author upon reasonable request.

References

[1] M.T. Dell'Anno, X. Wang, M. Onorati, M. Li, F. Talpo, Y. Sekine, S. Ma, F. Liu, W. B. Cafferty, N. Sestan, Human neuroepithelial stem cell regional specificity enables spinal cord repair through a relay circuit, Nat. Commun. 9 (1) (2018) 1–15.
[2] H. Liu, X. Xu, Y. Tu, K. Chen, L. Song, J. Zhai, S. Chen, L. Rong, L. Zhou, W. Wu, Engineering microenvironment for endogenous neural regeneration after spinal cord injury by reassembling extracellular matrix, ACS Appl. Mater. Interfaces 12 (15) (2020) 17207–17219.
[3] G. David, S. Mohammadi, A.R. Martin, J. Cohen-Adad, N. Weiskopf, A. Thompson, P. Freund, Traumatic and nontraumatic spinal cord injury: pathological insights from neuroimaging, Nat. Rev. Neurol. (2019) 1–14.
[4] Y. Jiang, P. Fu, Y. Liu, C. Wang, P. Zhao, X. Chu, X. Jiang, W. Yang, Y. Wu, Y. Wang, Near-infrared light-triggered NO release for spinal cord injury repair, Sci. Adv. 6 (39) (2020), eabc3513.
[5] D. Liu, J. Chen, T. Jiang, W. Li, Y. Huang, X. Lu, Z. Liu, W. Zhang, Z. Zhou, Q. Ding, Biodegradable spheres protect traumatically injured spinal cord by alleviating the glutamate-induced excitotoxicity, Adv. Mater. 30 (14) (2018) 1706032.
[6] J.L. Zou, S. Liu, J.H. Sun, W.H. Yang, Y.W. Xu, Z.L. Rao, B. Jiang, Q.T. Zhu, X. L. Liu, J.L. Wu, Peripheral nerve-derived matrix hydrogel promotes Remyelination and inhibits synapse formation, Adv. Funct. Mater. 28 (13) (2018) 1705739.
[7] A. Tay, A. Sohrabi, K. Poole, S. Seidlits, D. Di Carlo, A 3D magnetic hyaluronic acid hydrogel for magnetomechanical neuromodulation of primary dorsal root ganglion neurons, Adv. Mater. 30 (29) (2018) 1800927.
[8] Y. Zou, D. Ma, H. Shen, Y. Zhao, B. Xu, Y. Fan, Z. Sun, B. Chen, W. Xue, Y. Shi, Aligned collagen scaffold combination with human spinal cord-derived neural stem cells to improve spinal cord injury repair, Biomater. Sci. 8 (18) (2020) 5145–5156.
[9] A.J. Mothe, R.Y. Tam, T. Zahir, C.H. Tator, M.S. Shoichet, Repair of the injured spinal cord by transplantation of neural stem cells in a hyaluronan-based hydrogel, Biomaterials 34 (15) (2013) 3775–3783.
[10] A.R. Murphy, A. Laslett, C.M. O'Brien, N.R. Cameron, Scaffolds for 3D in vitro culture of neural lineage cells, Acta Biomater. 54 (2017) 1–20.
[11] A. Bakshi, O. Fisher, T. Dagci, B.T. Himes, I. Fischer, A. Lowman, Mechanically engineered hydrogel scaffolds for axonal growth and angiogenesis after transplantation in spinal cord injury, J. Neurosurg. Spine 1 (3) (2004) 322–329.
[12] C.D. Johnson, D. Ganguly, J.M. Zuidema, T.J. Cardinal, A.M. Ziemba, K.R. Kearns, S.M. McCarthy, D.M. Thompson, G. Ramanath, D.A. Borca-Tasciuc, Injectable, magnetically orienting electrospun fiber conduits for neuron guidance, ACS Appl. Mater. Interfaces 11 (1) (2018) 356–372.
[13] X. Li, C. Zhang, A.E. Haggerty, J. Yan, M. Lan, M. Seu, M. Yang, M.M. Marlow, I. Maldonado-Lasunción, B. Cho, The Effect of a Nanofiber-Hydrogel Composite on Neural Tissue Repair and Regeneration in the Contused Spinal Cord, Biomaterials, 2020, p. 119978.
[14] Y.-M. Kim, H.H. Park, D.H. Hwang, Y. Cui, E.M. Lee, S. Yahn, J.K. Lee, S.-C. Song, B.G. Kim, An injectable hydrogel enhances tissue repair after spinal cord injury by promoting extracellular matrix remodeling, Nat. Commun. 8 (1) (2017) 1–14.
[15] L.M. Marquardt, V.M. Doulames, A.T. Wang, K. Dubbin, R.A. Suhar, M. J. Kratochvil, Z.A. Medress, G.W. Plant, S.C. Heilshorn, Designer, injectable gels to prevent transplanted Schwann cell loss during spinal cord injury therapy, Sci. Adv. 6 (14) (2020), eaaz1039.
[16] E. Piantanida, G. Alonci, A. Bertucci, L. De Cola, Design of nanocomposite injectable hydrogels for minimally invasive surgery, Acc. Chem. Res. 52 (8) (2019) 2101–2112.
[17] Q. Feng, K.-y. Zhang, R. Li, L.-m. Bian, Injectable hydrogels for regenerative medicine, Acta Polym. Sin. (2021), 10.
[18] M.D. Baumann, C.E. Kang, C.H. Tator, M.S. Shoichet, Intrathecal delivery of a polymeric nanocomposite hydrogel after spinal cord injury, Biomaterials 31 (30) (2010) 7631–7639.
[19] M.D. Baumann, C.E. Kang, J.C. Stanwick, Y. Wang, H. Kim, Y. Lapitsky, M. S. Shoichet, An injectable drug delivery platform for sustained combination therapy, J. Contr. Release 138 (3) (2009) 205–213.
[20] G. Li, J. Wu, B. Wang, S. Yan, K. Zhang, J. Ding, J. Yin, Self-healing supramolecular self-assembled hydrogels based on poly (L-glutamic acid), Biomacromolecules 16 (11) (2015) 3508–3518.
[21] S. Li, M. Pei, T. Wan, H. Yang, S. Gu, Y. Tao, X. Liu, Y. Zhou, W. Xu, P. Xiao, Self-healing hyaluronic acid hydrogels based on dynamic Schiff base linkages as biomaterials, Carbohydr. Polym. 250 (2020) 116922.
[22] L. Li, B. Yan, J. Yang, L. Chen, H. Zeng, Novel mussel-inspired injectable self-healing hydrogel with anti-biofouling property, Adv. Mater. 27 (7) (2015) 1294–1299.
[23] S. Chen, S. Liu, L. Zhang, Q. Han, H. Liu, J. Shen, G. Li, L. Zhang, Y. Yang, Construction of injectable silk fibroin/polydopamine hydrogel for treatment of spinal cord injury, Chem. Eng. J. (2020) 125795.
[24] X. Liu, A.L. Miller, S. Park, B.E. Waletzki, Z. Zhou, A. Terzic, L. Lu, Functionalized carbon nanotube and graphene oxide embedded electrically conductive hydrogel synergistically timulates nerve cell differentiation, ACS Appl. Mater. Interfaces 9 (17) (2017) 14677–14690.
[25] L. Zhou, L. Fan, X. Yi, Z. Zhou, C. Liu, R. Fu, C. Dai, Z. Wang, X. Chen, P. Yu, Soft conducting polymer hydrogels cross-linked and doped by tannic acid for spinal cord injury repair, ACS Nano 12 (11) (2018) 10957–10967.
[26] K. Yue, G. Trujillo-de Santiago, M.M. Alvarez, A. Tamayol, N. Annabi, A. Khademhosseini, Synthesis, properties, and biomedical applications of gelatin methacryloyl (GelMA) hydrogels, Biomaterials 73 (2015) 254–271.
[27] U. Novak, A.H. Kaye, Extracellular matrix and the brain: components and function, J. Clin. Neurosci. 7 (4) (2000) 280–290.
[28] B. Meyer-Puttlitz, E. Junker, R.U. Margolis, R.K. Margolis, Chondroitin sulfate proteoglycans in the developing central nervous system. II. Immunocytochemical localization of neurocan and phosphacan, J. Comp. Neurol. 366 (1) (1996) 44–54.
[29] L. Zhou, G. Tan, K. Ouyang, Y. Liu, C. Ning, Highly water-dispersible, highly conductive, and biocompatible polypyrrole-coated silica particles stabilized and doped by chondroitin sulfate, Part. Part. Syst. Char. 32 (12) (2015) 1068–1077.
[30] T. Zahir, H. Nomura, X.D. Guo, H. Kim, C. Tator, C. Morshead, M. Shoichet, Bioengineering neural stem/progenitor cell-coated tubes for spinal cord injury repair, Cell Transplant. 17 (3) (2008) 245–254.
[31] Y. Yang, T.-T. Cao, Z.-M. Tian, H. Gao, H.-Q. Wen, M. Pang, W.-J. He, N.-X. Wang, Y.-Y. Chen, Y. Wang, Subarachnoid transplantation of human umbilical cord mesenchymal stem cell in rodent model with subacute incomplete spinal cord injury: preclinical safety and efficacy study, Exp. Cell Res. 395 (2) (2020) 112184.
[32] L. Zhou, L. Fan, F.-M. Zhang, Y. Jiang, M. Cai, C. Dai, Y.-A. Luo, L.-J. Tu, Z.-N. Zhou, X.-J. Li, Hybrid gelatin/oxidized chondroitin sulfate hydrogels incorporating bioactive glass nanoparticles with enhanced mechanical properties, mineralization, and osteogenic differentiation, Bioact. Mater. 6 (3) (2020) 890–904.
[33] L. Zhang, W.R. Stauffer, E.P. Jane, P.J. Sammak, X.T. Cui, Enhanced differentiation of embryonic and neural stem cells to neuronal fates on laminin peptides doped polypyrrole, Macromol. Biosci. 10 (12) (2010) 1456–1464.
[34] R. Bao, B. Tan, S. Liang, N. Zhang, W. Wang, W. Liu, A π-π conjugation-containing soft and conductive injectable polymer hydrogel highly efficiently rebuilds cardiac function after myocardial infarction, Biomaterials 122 (2017) 63–71.
[35] S. Hu, L. Zhou, L. Tu, C. Dai, L. Fan, K. Zhang, T. Yao, J. Chen, Z. Wang, J. Xing, Elastomeric conductive hybrid hydrogels with continuous conductive networks, J. Mater. Chem. B. 7 (15) (2019) 2389–2397.
[36] L. Fan, C. Liu, X. Chen, Y. Zou, Z. Zhou, C. Lin, G. Tan, L. Zhou, C. Ning, Q. Wang, Directing induced pluripotent stem cell derived neural stem cell fate with a three-dimensional biomimetic hydrogel for spinal cord injury repair, ACS Appl. Mater. Interfaces 10 (21) (2018) 17742–17755.
[37] A. Banerjee, M. Arha, S. Choudhary, R.S. Ashton, S.R. Bhatia, D.V. Schaffer, R. S. Kane, The influence of hydrogel modulus on the proliferation and differentiation of encapsulated neural stem cells, Biomaterials 30 (27) (2009) 4695–4699.
[38] C. Ning, L. Zhou, G. Tan, Fourth-generation biomedical materials, Mater. Today 19 (1) (2016) 2–3.
[39] L. Zhou, C. Dai, L. Fan, Y. Jiang, C. Liu, Z. Zhou, P. Guan, Y. Tian, J. Xing, X. Li, Injectable self-healing natural biopolymer-based hydrogel adhesive with thermoresponsive reversible adhesion for minimally invasive surgery, Adv. Funct. Mater. (2021) 2007457.

[40] X. Liu, J. Sun, Y. Yang, F. Zhou, Z. Pu, L. Li, Y. Zheng, Microstructure, mechanical properties, in vitro degradation behavior and hemocompatibility of novel Zn–Mg–Sr alloys as biodegradable metals, Mater. Lett. 162 (2016) 242–245.
[41] K.L. Ring, L.M. Tong, M.E. Balestra, R. Javier, Y. Andrews-Zwilling, G. Li, D. Walker, W.R. Zhang, A.C. Kreitzer, Y. Huang, Direct reprogramming of mouse and human fibroblasts into multipotent neural stem cells with a single factor, Cell stem cell 11 (1) (2012) 100–109.
[42] B.S. Eftekhari, M. Eskandari, P.A. Janmey, A. Samadikuchaksaraei, M. Gholipourmalekabadi, Surface topography and electrical signaling: single and synergistic effects on neural differentiation of stem cells, Adv. Funct. Mater. (2020) 1907792.
[43] D.M. Thompson, A.N. Koppes, J.G. Hardy, C.E. Schmidt, Electrical stimuli in the central nervous system microenvironment, Annu. Rev. Biomed. Eng. 16 (2014) 397–430.
[44] J.E. Collazos-Castro, G.R. Hernández-Labrado, J.L. Polo, C. García-Rama, N-Cadherin-and L1-functionalised conducting polymers for synergistic stimulation and guidance of neural cell growth, Biomaterials 34 (14) (2013) 3603–3617.
[45] Y. Xu, P.A. Patsis, S. Hauser, D. Voigt, R. Rothe, M. Günther, M. Cui, X. Yang, R. Wieduwild, K. Eckert, Cytocompatible, injectable, and electroconductive soft adhesives with hybrid covalent/noncovalent dynamic network, Adv. Sci. 6 (15) (2019) 1802077.
[46] C. Liu, L. Fan, J. Xing, Q. Wang, C. Lin, C. Liu, X. Deng, C. Ning, L. Zhou, L. Rong, Inhibition of astrocytic differentiation of transplanted neural stem cells by chondroitin sulfate methacrylate hydrogels for the repair of injured spinal cord, Biomater. Sci. 7 (5) (2019) 1995–2008.
[47] N.D. Jeffery, K. Brakel, M. Aceves, M.A. Hook, U.B. Jeffery, Variability in open-field locomotor scoring following force-defined spinal cord injury in rats: quantification and implications, Front Neuorl 11 (2020) 650.
[48] P. Lu, L.L. Jones, M.H. Tuszynski, Axon regeneration through scars and into sites of chronic spinal cord injury, Exp. Neurol. 203 (1) (2007) 8–21.
[49] W.-D. Lee, K.-C. Wang, Y.-F. Tsai, P.-C. Chou, L.-K. Tsai, C.-L. Chien, Subarachnoid hemorrhage promotes proliferation, differentiation, and migration of neural stem cells via BDNF upregulation, PloS One 11 (11) (2016), e0165460.
[50] T. Führmann, P.N. Anandakumaran, M.S. Shoichet, Combinatorial therapies after spinal cord injury: how can biomaterials help, Adv. Healthcare Mater. 6 (10) (2017) 1601130.
[51] H. Huang, H. Liu, R. Yan, M. Hu, PI3K/Akt and ERK/MAPK signaling promote different aspects of neuron survival and axonal regrowth following rat facial nerve axotomy, Neurochem. Res. 42 (12) (2017) 3515–3524.